Research Report

Personal Robot Assisting Transportation to Support Active Human Life: Posture Stabilization based on Zeroing Control Input of Actuator

Noriaki Hirose, Ryosuke Tajima, Kazutoshi Sukigara and Yuji Tsusaka

Report received on May 8, 2014

ABSTRACT This paper presents a personal robot (PR) that assists transportation in order to support active human lifestyles and proposes a novel posture control approach for the PR. At present, various PRs are being developed to support traveling in our aging society. Our PR can carry baggage and automatically follow a human being. Therefore, the PR can help a human being to walk outside with free hands to maintain their health. The high traveling performance of the PR is realized by control of the Zero Moment Point (ZMP). In this paper, the novel control method uses feedback compensation with an unstable pole to achieve the desired ZMP at steady state. To achieve the desired roll angle, the proposed controller changes the control input of the actuator of posture control to zero. The effectiveness of the proposed approach is verified via experiments using our first prototype of the PR.

KEYWORDS Personal Robot, Zero Moment Point, Posture Control, Unstable Pole, Active Aging

1. Introduction

Recently, various types of personal robots have been developed to support active lifestyles in our aging society.[1-3] However, excessive and premature robot support may accelerate the physical decline of elderly people. So, our research group proposes the personal robot (PR), which can carry baggage and automatically follow a human being. The owner of the PR can walk outside with empty hands even after shopping, and therefore supports an active, healthier lifestyle. Realizing the personal robot must satisfy two important issues:
(a) small footprint for coexistence with human beings,
(b) high traveling performance to follow the human being.

However, the small footprint causes a high center of gravity for the PR, which generally deteriorates the traveling performance of the PR. Therefore, it is difficult for the PR to realize both (a) and (b). To overcome these issues, the posture in some prototype PRs is controlled by actuators for the realization of the desired zero moment point (ZMP) in an actual environment. ZMP, which is the center of pressure for the floor reaction force, is used to evaluate the postural stability of the robot. Examples of our prototypes are shown in **Fig. 1**. Figure 1(a) is the first prototype PR developed in 2011.[4] This robot was used to design the basic structure of the posture control approach described in the following section. Figure 1(b) is the second prototype PR constructed in 2012[5] to improve the traversability by applying wheeled inverted pendulum control. Figure 1(c) is the latest prototype PR constructed in 2013.[6] This robot has a simple mechanical structure to reduce robot weight and provide storage space for baggage.

In this paper, the control approach for the roll angle[7-9] is discussed to improve the robustness for practical use.

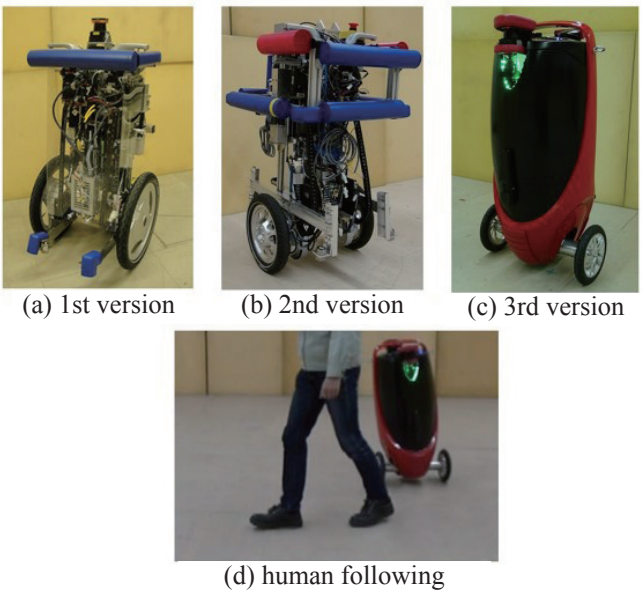

(a) 1st version (b) 2nd version (c) 3rd version

(d) human following

Fig. 1 Overview of the personal robot.

Posture control of the PR with regard to the roll angle should be required in the following cases:
(i) Quick turning around,
(ii) Movement over bumpy roads or slopes,
(iii) Application of an unknown and unmeasured disturbance force to the PR,
(iv) Fluctuation of the center of gravity of the PR.

In conventional research, a feedback control strategy using the roll angle is proposed for cases (i) and (ii).[10,11] In case (i), the posture should be controlled to the desired roll angle such that the centripetal acceleration is balanced by the acceleration of gravity. The reference angle for the desired roll angle can be calculated by estimating the centripetal acceleration from the angular velocity of the wheels. In case (ii), the posture angle can be controlled to the desired vertical posture by feedback control of the roll angle. However, fluctuation of tire pressure and variation of road surface conditions deteriorate the accuracy of the estimation of centripetal acceleration. As a result, the desired roll angle cannot be achieved, and the stability margin of the PR decreases. In addition, the conventional control approach cannot address cases (iii) and (iv). Furthermore, the estimated roll angle signal, which is the controlled variable for conventional feedback control, includes a detection error if the roll angle is not measured by a high-precision gyro sensor. This detection error also deteriorates the control performance and the stability margin of the PR. In the conventional approach, these factors cause the PR to overturn in some situations.

In the present paper, a novel control approach for posture stabilization is proposed to achieve the desired posture angle. The control input of the actuator for posture control (posture actuator) converges to zero to realize the desired posture in the proposed approach. The moment of the PR's own weight during the turning motion should balance the moment of the centrifugal force about the roll axis. To achieve the desired posture, the moment of the PR's own weight should also be balanced with the moment of the unknown disturbance force, for example, the force of wind, the fluctuation of the center of gravity, and the pushing force by a human being. On bumpy roads, the PR is required to maintain a vertical posture, as mentioned earlier. At the desired posture, the posture actuator does not need to generate a force to keep the desired posture in a steady state. Accordingly, the desired posture can be realized by zeroing the control input without a high-precision gyro sensor. In addition, the proposed approach also has an advantage with regard to energy consumption. However, it is difficult to both zero the control input and stabilize the control system by the conventional feedback compensation with stable poles and zeros because the plant system of the PR for roll motion is an unstable system.

In the present paper, a novel feedback compensation with an unstable pole is proposed to realize the desired posture by zeroing the control input. The experimental setup of the PR shown in Fig. 1(a) is first explained, and a simple mathematical model for roll motion is generated for the design of the proposed feedback compensation. The proposed control policy is then constructed by considering the relationship between the desired posture angle and the control input of the posture actuator. Finally, the proposed feedback compensation is designed, and the effectiveness of the proposed approach is verified experimentally by using the first prototype PR.

2. Experimental Setup and Mathematical Model

2. 1 Posture Actuator of Frst Prototype PR

The PR shown in Fig. 1(a) is equipped with two driving wheels in the front and one omnidirectional wheel in the rear. The PR, therefore, can move straight ahead and turn around by controlling the two driving wheels. However, posture control for the pitch angle and the roll angle is indispensable to achieve high acceleration and quick turning for the purpose of following a human being. To control the posture of the PR, the PR is equipped with posture actuators in the right and left wheels. **Figure 2**(a) shows a photograph of the posture actuator for the left wheel, which is constructed of a ball screw and a suspension, and Fig. 2(b) shows its mechanical structure. The purpose of the suspension is to suppress road noise in the higher frequency range, although in the present study, the spring of the suspension is rigid in order to evaluate the proposed control method. The roll moment τ to control the roll angle of the PR is appropriately expressed as follows:

$$\tau = -\frac{d}{2}\cdot F_R + \frac{d}{2}\cdot F_L, \tag{1}$$

where F_R is the force generated by the right ball screw, F_L is the force generated by the left ball screw,

and d (= 0.4) is the tread. In the present paper, the proposed approach is applied to the roll motion of the PR to evaluate its effectiveness. Therefore, the pitching motion is controlled by the conventional approach, in which the control variable is the pitch angle. On the other hand, the PR is equipped with an inertial measurement unit (IMU), which is composed of the triaxial gyro sensor and triaxial acceleration sensor, to control the posture angle.

2. 2 Motion Equation for the Roll Axis

Figure 3 is the front view of the kinematic model for the roll motion of the PR shown in Fig. 1(a). Here, J is the inertia of the PR about the roll axis, M is the weight of the PR, h is the height of the center of gravity, and θ is the roll angle. The PR is equipped with the gyro sensor to detect the angular velocity for roll $\dot{\theta}$. The motion equation about the roll axis is given as follows:

$$J\ddot{\theta} = \tau + hMg\sin\theta - hMv_m\omega_m\cos\theta, \tag{2}$$

where v_m is the translational velocity of the PR, ω_m is the turning angular velocity of the PR, and g is the acceleration of gravity. The second term of the right-hand side in Eq. (2) is the roll moment of the PR's own weight, and the third term of the right-hand side in Eq. (2) is the roll moment of the centrifugal force. Equation (2) can be linearized under the assumption $\theta << 1$ by substituting $\sin\theta = \theta$ and $\cos\theta = 1$.

$$J\ddot{\theta} = \tau + hMg\theta - hMv_m\omega_m \tag{3}$$

Equation (3) can be modified by Laplace transformation as follows:

$$\begin{aligned}\dot{\theta}(s) &= \frac{s}{Js^2 - hMg}\left(\tau(s) + hF(s)\right), \\ &= P(s)\left(\tau(s) + hF(s)\right),\end{aligned} \tag{4}$$

where F is the centrifugal force $Mv_m\omega_m$. From Eq. (4), the plant system $P(s)$ is verified to include an unstable pole.

3. Relationship between Actuator Torque and Desired Posture Angle

In this section, the relationship between the control input of the posture actuator and the desired posture angle is discussed for the case in which an unknown disturbance force is applied to the PR. Here, the unknown disturbance force is assumed to be a centrifugal force, a force of the wind, a fluctuation of the center of gravity, or a pushing force by a human being. **Figure 4**(a) shows one example controlled by the conventional method when unknown force F_d is applied to the upper body of the PR. In Fig. 4(a), the current posture angle is shown as 0 degrees. The conventional control method generates the following control input τ to maintain the current posture angle, because the control variable in the conventional method is the roll angle.

$$\tau = F_d h\cos\theta - hMg\sin\theta \tag{5}$$

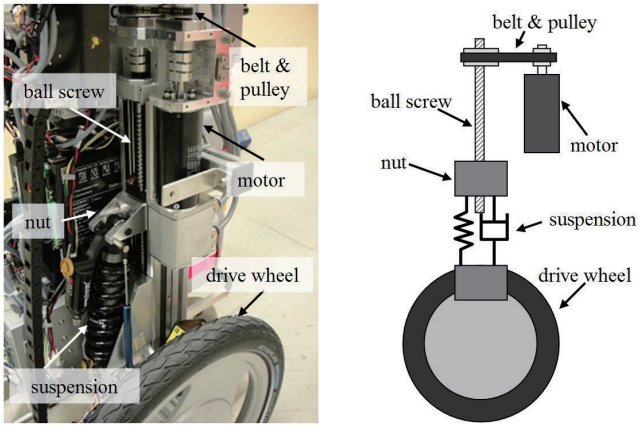

(a) photograph (b) configuration

Fig. 2 Left side actuator of the Personal Robot.

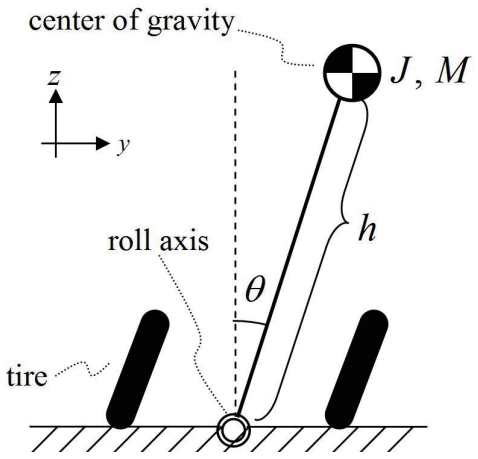

Fig. 3 Configuration of model for rolling motion.

Although the control input τ in Eq. (5) can maintain the PR's posture, the ZMP (red point in Fig. 4) fluctuates. The decrease in the stability margin is confirmed through comparison to the case without F_d, as shown in Fig. 4(b). To realize the desired ZMP when F_d is applied, the following posture angle θ should be achieved as in Fig. 4(c).

$$\theta = \tan^{-1}\frac{F_d}{Mg} \tag{6}$$

From Fig. 4(c), the control input should be zero in the desired posture, because the roll moment of the PR's own weight Mg can balance the roll moment of the unknown disturbance force F_d. The actuator torque τ in Eq. (5) is zero by substituting Eq. (6) into Eq. (5). In the proposed approach, the desired posture angle is achieved by zeroing the control input.

4. Proposed Control Method

4. 1 Design Approach of Feedback Compensation

The desired posture shown in Fig. 4(c) can be achieved by the following conditions:
(a) Stabilize the feedback control system for angular velocity about the roll axis,
(b) Converge the control input to zero in the steady state.

For (a) and (b), the feedback control system shown in **Fig. 5** is simply designed. Here, $C(s)$ is the proposed feedback compensation, τ_{dis} is the roll moment generated by the unknown disturbance force F_d, and $\dot{\theta}_{ref} = 0$ is the reference of $\dot{\theta}$. As shown in Section 2.2, the plant system $P(s)$ includes an unstable pole. Therefore, to satisfy condition (a), the Nyquist locus $P(j\omega)C(j\omega)$ for $-\infty < \omega < \infty$ should rotate counterclockwise once at $[-1,\ j0]$ on the Nyquist diagram under the assumption that $C(s)$ is designed by the stable poles and the stable zeros. The Nyquist locus for $0 < \omega < \infty$ and the Nyquist locus for $-\infty < \omega < 0$ are symmetric about the real axis. Therefore, the Nyquist locus at $\omega = 0$ should be on the real axis and to the left side of $[-1,\ j0]$ to achieve condition (a).

On the other hand, the gain characteristic of $\frac{\tau}{\tau_{dis}}$ should be $-\infty$ at $\omega = 0$ to achieve condition (b). The transfer function $\frac{\tau}{\tau_{dis}}$ is shown as follows:

$$\frac{\tau(s)}{\tau_{dis}(s)} = \frac{-P(s)C(s)}{1+P(s)C(s)}. \tag{7}$$

To consider (b) with (a), the gain characteristic of $\frac{-P(s)C(s)}{1+P(s)C(s)}$ is plotted on the Nyquist diagram shown in **Fig. 6**. In Fig. 6, the red region indicates the high gain of $\frac{-P(s)C(s)}{1+P(s)C(s)}$, and the blue region indicates the low gain of $\frac{-P(s)C(s)}{1+P(s)C(s)}$. Therefore, the Nyquist locus at $\omega = 0$ should be drawn around the original point $[0,\ j0]$ to satisfy condition (b). On the other hand, to avoid the spill-over phenomenon, the Nyquist locus at the higher frequency range must also be drawn around the original point $[0,\ j0]$.

As a result, conditions (a) and (b) cannot be achieved simultaneously under the conventional design policy of feedback compensation using stable poles and zeros. Therefore, feedback compensation with one unstable pole is proposed to realize both (a) and (b). The open-loop transfer function $P(s)C(s)$ has two unstable poles, if the feedback controller $C(s)$ includes one unstable

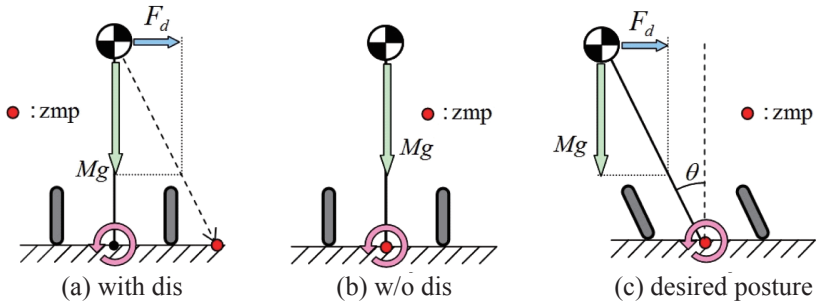

Fig. 4 Behavior with and without disturbance.

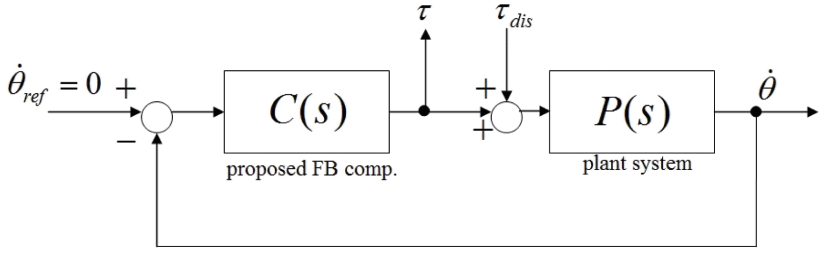

Fig. 5 Block diagram for control system.

pole. Therefore, the Nyquist locus for $-\infty < \omega < \infty$ should rotate counterclockwise twice at $[-1,\ j0]$ to stabilize the control system. In other words, the Nyquist locus for $0 < \omega < \infty$ should rotate counterclockwise once at $[-1,\ j0]$. This means that the Nyquist locus at $\omega = 0$ can be drawn on the original point $[0,\ j0]$ to achieve (b) with (a).

4. 2 Design of Feedback Compensation with an Unstable Pole

Figure 7 shows the frequency characteristic of plant system $P(s)$. Here, J is 12.8, M is 41.5, and h is 0.5. The gain characteristic of $P(s)$ is 20 dB/dec under 0.7 Hz and –20 dB/dec over 0.7 Hz. The phase characteristic of $P(s)$ is –90 degrees over the entire frequency band. As mentioned earlier, the Nyquist locus for $0 < \omega < \infty$ should rotate counterclockwise once at $[-1,\ j0]$, and the Nyquist locus at $\omega = 0$ and $\omega = \infty$ should be $[0,\ j0]$. The counterclockwise rotation of the Nyquist locus is achieved as follows. The phase characteristic of $P(s)C(s)$ has a phase-lead element of +180 degrees from –270 degrees, and the gain characteristic of $P(s)C(s)$ has a gain peak that is like the peak from a bandpass filter.

It is confirmed that the gain characteristic of $P(s)$ is satisfied by the desired gain characteristic of $P(s)C(s)$ Therefore, the proposed feedback compensation $C(s)$ is designed by considering the required phase characteristic for $P(s)C(s)$, as follows:

$$C(s) = K_c \cdot \frac{s+\omega_1}{\omega_1} \cdot \frac{-\omega_2}{s-\omega_2}, \tag{8}$$

where each parameter K_c, ω_1, and ω_2 is designed as follows.

To realize –270 degrees of $P(s)C(s)$ at $\omega = 0$, K_c is designed as the negative value –30. Therefore, the phase characteristic of $P(s)C(s)$ at $\omega = 0$ is –270 degrees, because the phase value of $P(s)$ is –90 degrees and the phase value of $C(s)$ at $\omega = 0$ is –180 degrees. On the other hand, $C(s)$ is required to have the phase-lead element of +180 degrees for counterclockwise rotation of the Nyquist locus. Here, $C(s)$ includes the phase-lead compensation $\frac{s+\omega_1}{\omega_1}$ of $\omega_1 = 2 \cdot \pi \cdot 0.5$ and the unstable pole $\frac{-\omega_2}{s-\omega_2}$ of $\omega_2 = 2 \cdot \pi \cdot 15.0$.

These compensations can achieve the phase-lead element of +180 degrees. **Figure 8** shows the frequency characteristic of $C(s)$. In Fig. 8, the desired phase characteristic is achieved by using an unstable pole.

The Nyquist diagram of the proposed feedback compensation is shown in **Fig. 9**. The Nyquist locus for $0 < \omega < \infty$ can successfully rotate counterclockwise once at $[-1,\ j0]$ and the Nyquist locus at $\omega = 0$ and $\omega = \infty$ is at $[0,\ j0]$. In addition, the sufficient gain margin and phase margin are confirmed to realize the robustness of the control system. **Figure 10** shows the gain characteristic of $\frac{-P(s)C(s)}{1+P(s)C(s)}$. From Fig. 10, the gain at the lower frequency range is attenuated to achieve zeroing of the control input in the steady state.

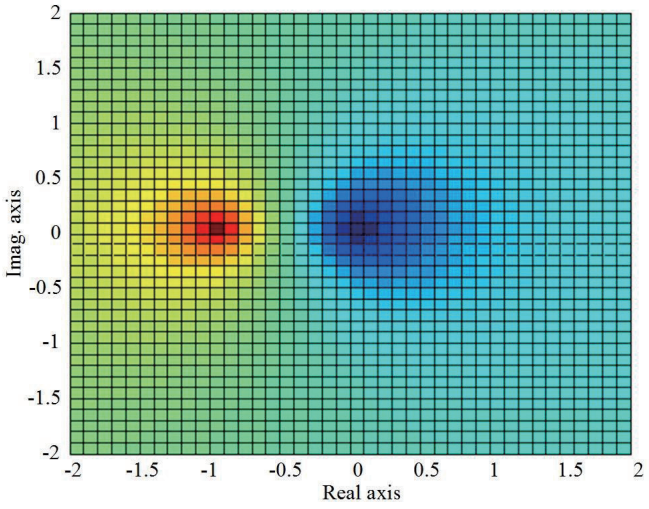

Fig. 6 Gain characteristics of $\frac{-P(s)C(s)}{1+P(s)C(s)}$ on Nyquist diagram.

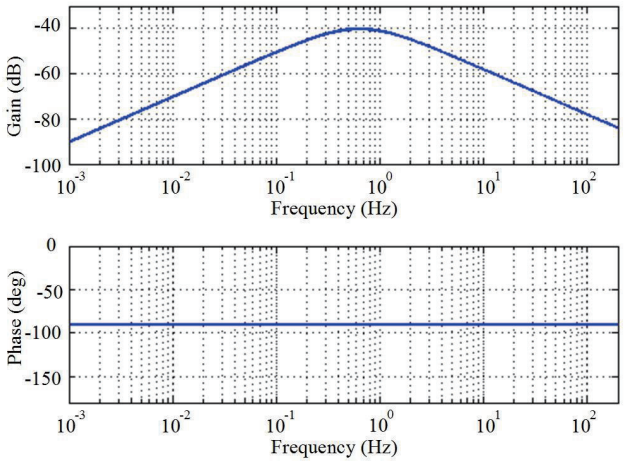

Fig. 7 Frequency characteristics of plant system $P(s)$.

5. Experimental Results

Figure 11 is a block diagram of the proposed control system with additional compensations to deal with the Coulomb friction of the posture actuator. The Coulomb friction force τ_{cdis} essentially deteriorates the control performance of the proposed approach. In the experiment, the additional input τ_c, which cancels τ_{cdis}, and the dither input $\dot{\theta}_{dith}$ are applied to improve the deteriorated performance. In this section, the subject of the proposed approach in the experiment is first explained, and the additional compensations τ_c and $\dot{\theta}_{dith}$ are applied to the proposed control system. Then, the effectiveness of the proposed approach is experimentally verified by the turning motion.

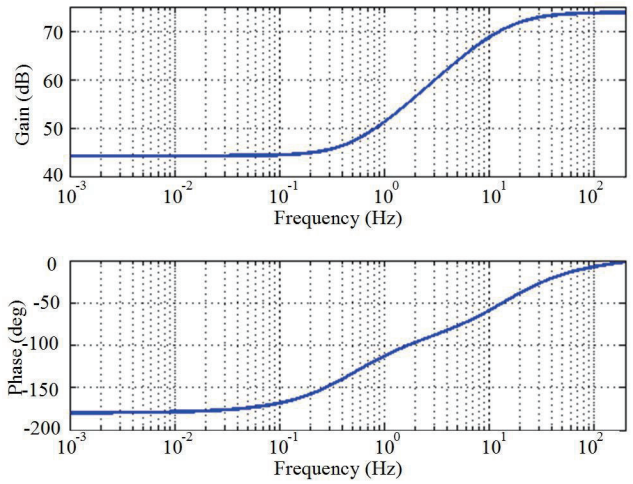

Fig. 8 Frequency characteristics of FB compensation $C(s)$.

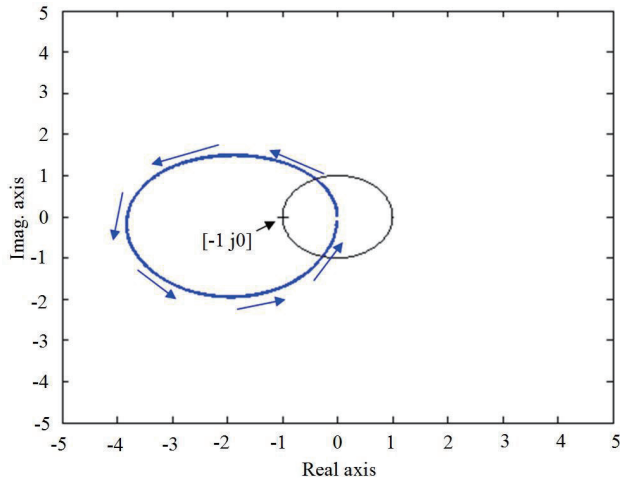

Fig. 9 Nyquist diagram.

5. 1 Friction Compensation for the Proposed Approach

Figure 12 shows the experimental results without the additional compensations when the velocity references for the driving wheels are 0. In Fig. 12, (a) shows the roll angle and (b) shows the control input of the posture actuator. In Fig. 12(b), the red line is the raw control input (blue line) with noise removed via a low-pass filter. The roll angle causes an oscillating motion between 0.07 rad and –0.08 rad. On the other hand, the control input is controlled to zero when the roll angle is 0.07 rad and –0.08 rad. The Coulomb friction τ_{cdis} of the posture actuator causes this oscillating motion because the proposed feedback compensation controls the roll angle to an undesired value, which the moment of the PR's own weight balances by the friction torque in order to zero the control input.

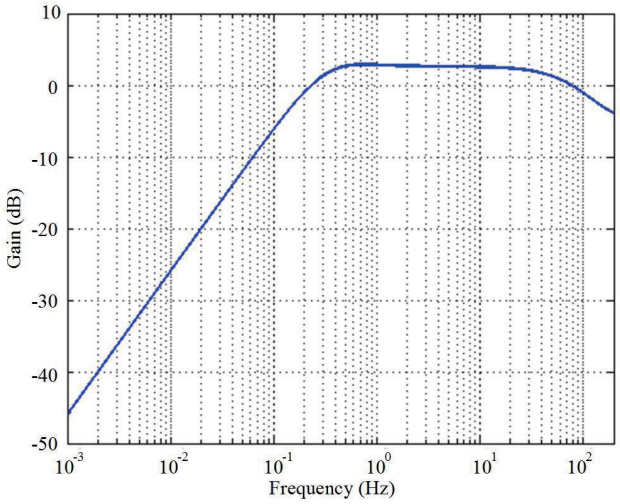

Fig. 10 Gain Characteristics of $\frac{-P(s)C(s)}{1+P(s)C(s)}$.

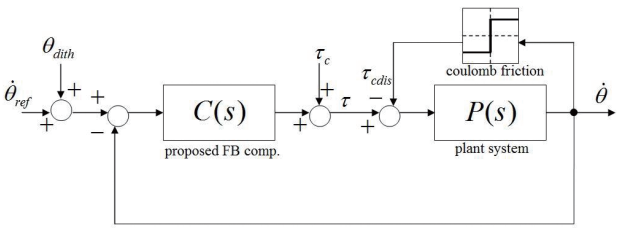

Fig. 11 Block diagram of the proposed control system with additional compensation for experiment.

To solve this problem in the experiment, the dither input $\dot{\theta}_{dith}$ and the friction compensation τ_c are superimposed on the reference of the angular velocity $\dot{\theta}_{ref}$ and the output of the feedback compensation $C(s)$, respectively. Here, $\dot{\theta}_{dith}$ and τ_c are designed by trial and error as follows:

$$\dot{\theta}_{dith}(t) = 0.075 \cdot \sin(2 \cdot \pi \cdot 10 \cdot t), \tag{9}$$

$$\tau_c(t) = \begin{cases} 18 & (\dot{\theta}(t) > 0.005) \\ \dfrac{18}{0.005} \cdot \dot{\theta}(t) & (|\dot{\theta}(t)| \le 0.005) \\ -18 & (\dot{\theta}(t) < -0.005) \end{cases}. \tag{10}$$

Figure 13 shows the experimental results with the dither input $\dot{\theta}_{dith}$ and friction compensation τ_c. The roll angle is controlled to 0 degrees, and the steady component of the control input is set to 0. However, these compensations are not suitable for practical use from the viewpoint of the stability margin and energy consumption. Therefore, $\dot{\theta}_{dith}$ and τ_c are applied only to evaluate the effectiveness of the proposed approach.

5. 2 Experimental Results of Turning Motion

Figure 14 shows the angular velocity of the right and left wheels for the turning motion. The PR can perform steady turning motion between 4.0 s and 8.0 s, as indicated by the vertical dotted lines. In this experiment, the centrifugal force during the turning motion is assumed as unknown disturbance force F_d to evaluate the proposed approach. The experimental results of the roll angle and the control input are shown in **Figs. 15**(a) and (b), respectively. From Fig. 15(a), the roll angle can be controlled to the desired steady value during the turning motion indicated by the vertical dotted line. In addition, the steady component of the control input shown in Fig. 15(b) is set to 0 during the turning motion, because the moment of the unknown centrifugal force can balance the moment of the PR's own weight. **Figure 16** is a snapshot of the PR during the steady turning of Fig. 15. From Fig. 16, tilting the upper body of the PR can be clearly confirmed. The lifter behind the PR is used only for safety to prevent a runaway or a rollover in the experiment.

The merits of the proposed approach are clearly presented without comparison, because the roll angle cannot be controlled in the conventional method under the same experimental condition. The experiments in Fig. 15 are performed under the condition that the centrifugal force is unknown and desired roll angle cannot be calculated by Eq. (6).

5. 3 Analysis of the ZMP Trajectory

The ZMP trajectory cannot be verified experimentally, because the floor reaction force cannot be observed in the experiment. To analyze the ZMP trajectory, the multibody dynamics model shown in **Fig. 17** is designed by 3D CAD drawing sheets, and the motion of the model is constrained by the experimental data of Fig. 15. As a result of the numerical analysis, the floor reaction force can be obtained, and the calculated ZMP trajectory for the y-axis is shown in **Fig. 18**.

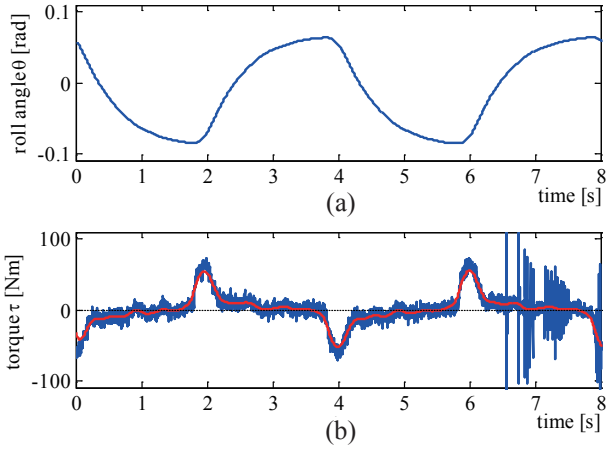

Fig. 12 Experimental results for the proposed control.

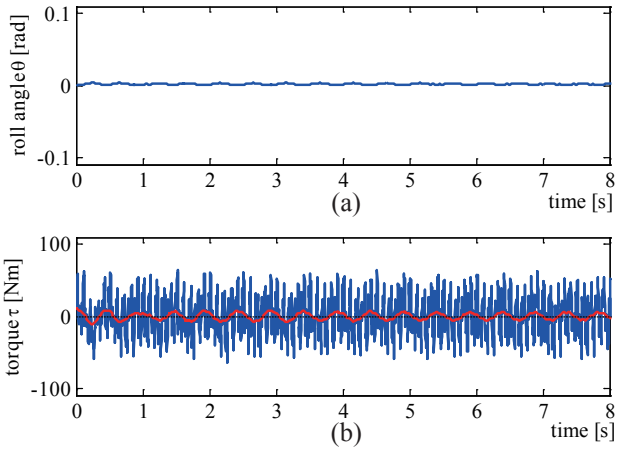

Fig. 13 Experimental results for the proposed control with τ_c and $\dot{\theta}_{dith}$.

The ZMP trajectory during the steady turning motion indicated by the vertical dotted line is within ±0.01 m. These results indicate that the PR can achieve the desired posture angle and ensure the stability margin during the turning motion. The effectiveness of the proposed approach can be verified experimentally and analytically by the multibody dynamics model.

6. Conclusion

In the present paper, a novel feedback control approach was proposed to control the posture angle in the personal robot. The proposed feedback compensation with an unstable pole realized the appropriate posture angle to achieve quick turning and ensure the stability margin for an unknown disturbance force. In the experiments, the roll angle was controlled to the desired angle by zeroing the control input of the posture actuator. Although the effectiveness of the proposed approach was verified experimentally by using the first prototype PR, the proposed approach can be applied to other robots having a posture actuator.

Future work is improvement of the stability margin in the transient state. The ZMP trajectory (Fig. 18)

Fig. 16 Snapshot of the PR during steady turning.

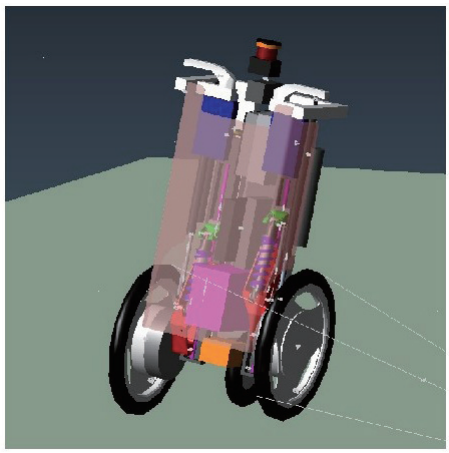

Fig. 17 Configuration of multibody dynamics model.

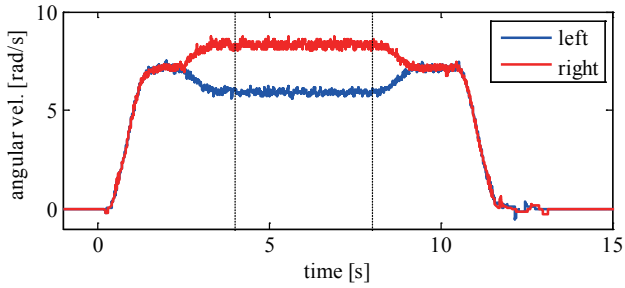

Fig. 14 Angular velocity of right and left wheels.

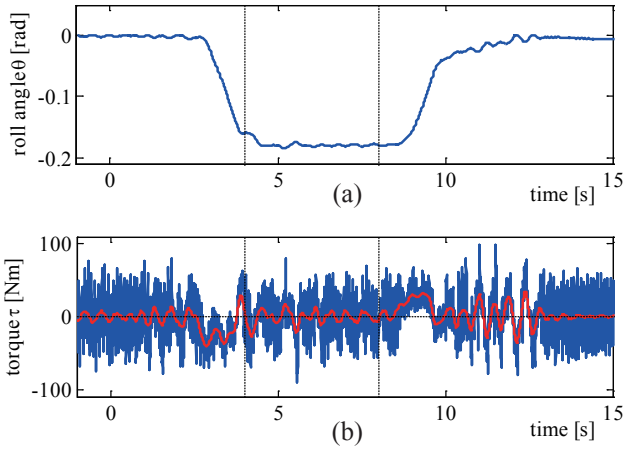

Fig. 15 Experimental results for turning motion.

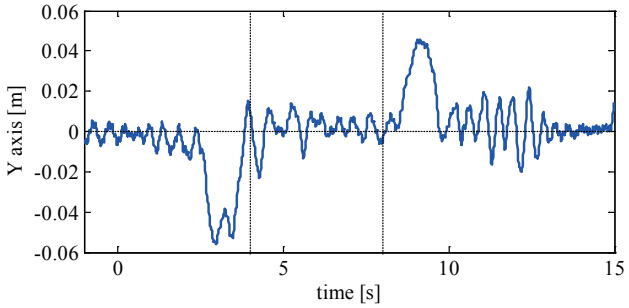

Fig. 18 ZMP trajectory of *Y* axis.

produces overshoot and undershoot at approximately 3.0 s and 9.0 s, respectively, because the angular acceleration around roll axis is occurred to realize the desired posture by the proposed approach. To suppress the fluctuation of the ZMP trajectory in the transient state, a predictive control approach with ZMP constraints will be required.[12]

References

(1) Yamaoka, M., "Personal Mobility Robot", *J. of the Robotics Soc. of Japan* (in Japanese), Vol. 26, No. 8 (2008), pp. 885-886.

(2) Hirose, N. et al., "Mode Switching Control for a Personal Mobility Robot based on Initial Value Compensation", *Proc. of the 36th Annu. Conf. of the IEEE Industrial Electronics Soc.* (2010), pp. 1908-1913.

(3) Hirose, N. et al., "Suppression of Roll Vibration for Personal Mobility Robot using Driving Torque of Wheels", *Proc. of the 2012 IEEE Int. Conf. on Industrial Tech.* (2012), pp. 154-159.

(4) Hirose, N. et al., "Posture Stabilization for a Personal Mobility Robot using Feedback Compensation with an Unstable Pole", P*roc. of the 2013 IEEE Int. Conf. on Mechatronics* (2013), pp. 804-809.

(5) Hirose, N. et al., "*Hitonami no Undouseinou wo Yuusuru Kogataidoutai no Jitsugen*: *Daisanpou Yokokasokudo wo Mochiita Shiseianteikaseigyo*", *Proc. of the 30th Annu. Conf. of the Robotics Soc. of Japan* (in Japanese), (2012), RSJ2012AC1G2-1.

(6) Hirose, N. et al., "Personal Robot Assisting Transportation to Support Active Human Life -Posture Stabilization Based on Feedback Compensation of Lateral Acceleration-", *Proc. of the 2013 IEEE/RSJ Int. Conf. on Intelligent Robots and Systems* (2013), pp. 659-664.

(7) Hibbard, R. and Karnopp, D., "Methods of Controlling the Lean Angle of Tilting Vehicles", *Advanced Automotive Tech.*, Vol. 52, (1993), pp. 311-320.

(8) Hibbard, R. and Karnopp, D., "Twenty-First Century Transportation System Solutions: A New Type of Small, Relatively Tall and Narrow Active Tilting Commuter Vehicle", *Vehicle System Dynamics*, Vol. 25, No. 5 (1996), pp. 321-347.

(9) Krid, M. and Benamar, F., "Design and control of an active anti-roll system for a fast rover", P*roc. of the 2011 IEEE/RSJ Int. Conf. on Intelligent Robots and Systems* (2011), pp. 274-279.

(10) Rajamani, R. et al., "Dynamics of Narrow Tilting Vehicles", *Mathematical and Computer Modeling of Dynamical Systems*, Vol. 9, No. 2 (2003), pp. 209-231.

(11) Nakamura, R. et al., "Study on Traveling Method on Rough Terrain for 2-Wheels Inverted Pendulum with Hybrid Suspensions", *Proc. of the 15th Robotics Symposia* (in Japanese), (2010), pp. 303-308.

(12) Hirose, N. et al., "Personal Robot Assisting Transportation to Support Active Human LIfe -Reference Generation based on Model Predictive Control for Robust Quick Turning-", *Proc. of the 2014 IEEE Int. Conf. on Robotics & Automation* (2014), pp. 2223-2230.

Noriaki Hirose
Research Field:
- Motion Control

Academic Degree: Dr.Eng.
Academic Societies:
- The Institute of Electrical Engineers of Japan
- The Robotics Society of Japan
- The Japan Society of Mechanical Engineers

Award:
- Young Investigator Excellence Award, The Robotics Society of Japan, 2013

Ryosuke Tajima
Research Field:
-Robotics

Academic Degree: Dr.Eng.
Academic Society:
- The Robotics Society of Japan

Award:
- Young Investigator Excellence Award, The Robotics Society of Japan, 2009

Kazutoshi Sukigara
Research Field:
-Development of Personal Robot

Yuji Tsusaka
Research Field:
-Development of Path Planning and Control for Industrial and Partner Robot

Academic Degree: Dr.Eng.
Academic Societies:
-The Robotics Society of Japan
-The Japan Society of Mechanical Engineers

